TERMINAL-LEVEL RELAXATION IN ND-DOPED LASER MATERIALS

C. Bibeau

S. A. Payne

Introduction

During the energy extraction of a 1-µm pulse in a Nd-doped laser material, the Nd-ion population is transferred from the metastable $^4F_{3/2}$ level into the terminal $^4I_{11/2}$ level, as shown in Fig. 1. The *terminal-level lifetime*, $\tau_{11/2}$, is defined in this case as the time it takes the Nd-ion population to decay from the $^4I_{11/2}$ level into the $^4I_{9/2}$ ground state. Several experimental and theoretical approaches over the last three decades have been made to measure the terminal-level lifetime. However, an agreement in the results among the different approaches for a large sampling of laser materials has never been demonstrated.

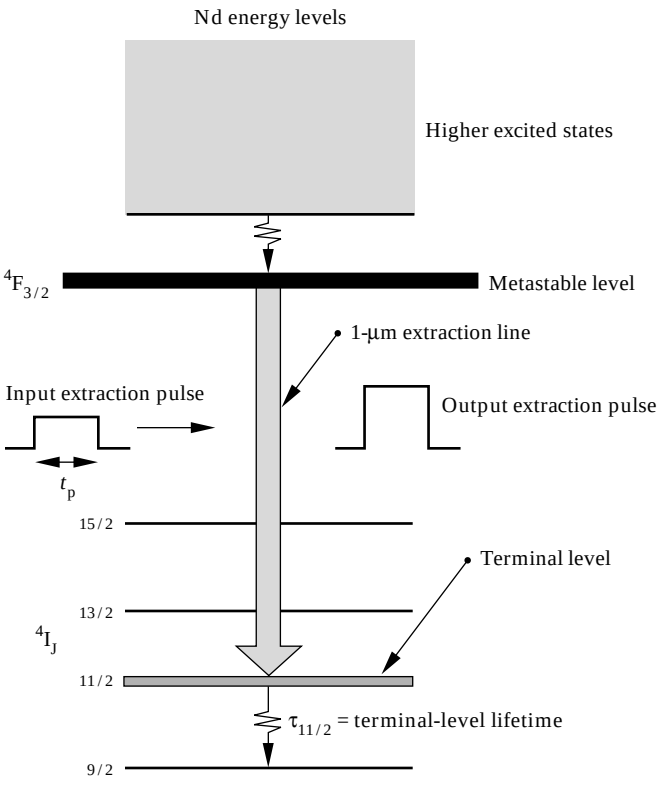

FIGURE 1. A Nd^{3+} energy level diagram that shows the 1-µm laser transition from the $^4F_{3/2}$ metastable level into the $^4I_{11/2}$ terminal level. During this transition, the input extraction pulse is amplified to produce a more energetic output pulse. The nonradiative relaxation from the $^4I_{11/2}$ level into the $^4I_{9/2}$ ground state is known as the terminal-level lifetime ($\tau_{11/2}$). (70-15-0993-3196pb01)

This article presents three independent methods (pump-probe, emission, and energy extraction) for measuring the terminal-level lifetime in Nd:phosphate glass LG-750. We find remarkable agreement among the data and determine the $\tau_{11/2}$ lifetime to be 253 ± 50 ps. We extend our studies to show that the results of the pump-probe and emission methods agree to within a factor of two for additional Nd-doped glasses and crystals investigated, thus offering validation for the emission method, which is a simpler, indirect approach.

Background

As explained, $\tau_{11/2}$ is the time it takes the Nd-ion population to decay from the $^4I_{11/2}$ level into the $^4I_{9/2}$ ground state during the energy extraction of a 1-µm pulse. If the decay time is infinitely fast compared with the length of the extraction pulse ($\tau_{11/2} << t_p$) then the $^4I_{11/2}$ level will appear to be virtually unpopulated for the duration of the extraction pulse. Since the small signal gain coefficient (g_0) is directly proportional to the population inversion (ΔN) between the upper $^4F_{3/2}$ level and the lower $^4I_{11/2}$ level, the incoming laser pulse will extract more of the stored energy if the $^4I_{11/2}$ level remains unpopulated. Conversely, if the length of the extracting pulse is much less than the terminal-level lifetime ($t_p << \tau_{11/2}$) then the population in the $^4I_{11/2}$ level will remain populated or bottlenecked. As a consequence, the extraction process will be less efficient

since stimulated emission and absorption processes can become competitive and thus cause the re-excitation of the Nd-ion population in the $^4I_{11/2}$ level back into the $^4F_{3/2}$ level during extraction.

Figure 2 is a plot of the ideal extraction efficiency for Nd:phosphate glass as a function of the ratio $R = t_p / \tau_{11/2}$. For comparison, a few additional data are shown, including the oxide crystals Nd:YAG and Nd:YALO and the fluoride crystal Nd:YLF. The data points for these materials do not lie exactly on the phosphate curve due to differences in the spacing of the energy levels that affect the degeneracies of the upper and lower laser levels and thus the values for the extraction efficiency. The pulse lengths are assumed to be square in shape with a length of 3 ns, with the exception of the National Ignition Facility (NIF) data point, where t_p is 8 ns. The proposed design of the NIF will use a Nd-doped phosphate glass similar to LG-750 and will require longer pulse lengths. We discuss a derivation of this curve in a later section, but for now it illustrates that the extraction efficiencies for a Nd:phosphate glass laser are only moderately impacted by the short terminal lifetime (< 1 ns), whereas for Nd:YLF the long terminal lifetime (~10 ns) can become a limiting factor.

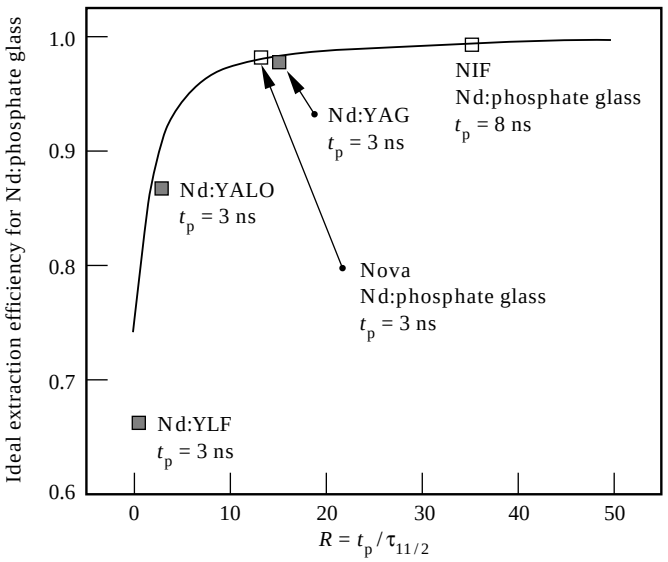

FIGURE 2. The ideal extraction efficiency plotted as a function of the ratio of the pulse length t_p to the terminal-level lifetime $\tau_{11/2}$ for Nd:phosphate glass. For comparison, additional data are shown (solid squares). The plots illustrate that the relatively short terminal lifetimes (<1 ns) of the phosphate glass used in the Nova laser and of the glass used in the design of the NIF are not a limiting factor in obtaining the highest possible extraction efficiency. In comparison, the long lifetime (~10 ns) of the fluoride crystal, Nd:YLF, can be a limiting factor. (70-00-0295-0392pb01)

Given the importance of the terminal-level lifetime for phosphate glass, we employ three different methods for measuring its value. We first describe a novel and more accurate direct approach that employs a pump-probe technique.[1] We also explore an indirect emission method, which is based on the "energy-gap law,"[2,3] since this method continues to be the preferred method due to its simple and straightforward approach. However, it is a method that presupposes that the lifetime of a different nonradiative transition ($^4G_{7/2} \rightarrow {}^4G_{5/2}, {}^2G_{7/2}$), whose energy gap coincidentally matches that of the relevant transition ($^4I_{11/2} \rightarrow {}^4I_{9/2}$), provides a reasonable assessment of the actual terminal-level lifetime. Based on the validity of the energy gap law, the two lifetimes are expected to be equal. Finally, we model data taken from a previous set of experiments and show that the terminal lifetime for phosphate glass derived from the best fit to the data is in agreement with the values derived from the pump-probe and indirect emission experiments.

In addition, we found in the process of modeling the extraction data that it would be useful if an approximate solution of the energy transport and kinetic differential equations existed that explicitly include the terminal lifetime and the pulse length. The motivation for finding an empirical solution was to be able to use a simple expression within the existing models that would include the effects of the terminal-level lifetime without having to tediously integrate the energy transport and kinetic differential equations. To date, the only analytic solutions that exist are for the two extreme cases of $t_p / \tau_{11/2} << 1$ and $t_p / \tau_{11/2} >> 1$, that is, very short or long pulse lengths relative to the terminal lifetime.[4] We formulated an empirical solution of the saturation fluence that explicitly includes the ratio $t_p / \tau_{11/2}$ and is therefore valid in the intermediate region of $t_p / \tau_{11/2} \approx 1$ as well. Our empirical solution of the saturation fluence can be substituted within the well known Frantz–Nodvik[4] analytic solution to model the energy extracted from an amplifier. We present a modified expression for the saturation fluence and describe how we used it to model the energy extraction data for Nd:phosphate glass.

We first describe the direct (pump-probe) method followed by the indirect (fluorescence) method and discuss the lifetime results for LG-750. Next, we model the extraction data previously taken by Yarema and Milam[5] and discuss our model. We show concurrence among the three methods with an averaged lifetime of $\tau_{11/2}$ = 253 ps with an rms error of ±50 ps. In the final section we compare the results from the direct and indirect methods for 13 materials and show that the simpler, indirect method can be used to determine the terminal lifetimes with an uncertainty of less than a factor of two in most circumstances.

Direct Method: Experiment and Results

To directly measure the population decay time between two electronic levels of interest, we must first find a way to selectively populate the upper level and then be able to detect and accurately measure the population decay. The total decay rate of the emission signal is a sum of the radiative and nonradiative decay rates. In most Nd-doped hosts, the small energy gap (<1500 cm^{-1}) of the $^4I_{11/2} \rightarrow {}^4I_{9/2}$ transition and high phonon frequencies (up to 1300 cm^{-1}) enable the nonradiative rate to be much faster than the radiative rate. This causes the photon emission signal from the $^4I_{11/2}$ level to be very weak, thus making an accurate measurement of the nonradiative lifetime inherently difficult. Until recently, many of the direct measurements employed either an energy-extraction or gain-recovery method coupled with a numerical model.[6,7]

We designed a unique pump-probe experimental technique to directly measure the nonradiative lifetime for the $^4I_{11/2} \rightarrow {}^4I_{9/2}$ transition in various Nd-doped glasses and crystals. Figure 3 shows a series of energy level diagrams describing the sequence of events for the experiment: (1) A 2.41-µm pump beam excites a fraction of the ground state Nd ions into the $^4I_{13/2}$ level, after which the Nd ions will nonradiatively decay into the $^4I_{11/2}$ level. (2) After an incremental time delay, a 1.06-µm probe beam excites a fraction of the $^4I_{11/2}$ population into the $^4F_{3/2}$ level. (3) The $^4F_{3/2}$ population can decay into several of the lower ^4I_J levels, but we chose to record the 0.88-µm emission signal corresponding to the $^4F_{3/2} \rightarrow {}^4I_{9/2}$ transition. The time-integrated 0.88-µm signal is proportional to the $^4I_{11/2}$ population. This sequence of events is repeated for each increased time delay between the pump and probe pulses. Therefore, as the time delay between the pump and probe pulses increases, the value of the integrated 0.88-µm emission signal diminishes since most of the $^4I_{11/2}$ population will eventually return into the ground state. A plot of the *time-integrated* 0.88-µm emission values vs time delay (τ_d) will construct the temporal evolution of the $^4I_{11/2}$ population. In passing we note that directly populating the $^4I_{11/2}$ level can be difficult due to the increased intrinsic absorption of the host medium at 5 µm.

Figure 4 shows a simplified experimental diagram. The 1.06-µm output of a mode-locked laser operating at a repetition rate of 76 MHz is injected into a regenerative amplifier. The output pulses emerge from the amplifier at a 10-Hz repetition rate with an energy of 55 mJ per pulse. Two nonlinear frequency conversion processes are required to generate the 2.41-µm pump beam: a Raman process to generate 1.91-µm output and a difference frequency generator to produce the 2.41-µm output. The 1.06-µm pulse is split with a beam splitter that allows 80% of the 1.06-µm energy to pass through a high-pressure (55-atm) Raman cell filled with H_2. The 1.06-µm beam excites several vibrational modes of the H_2 molecules, allowing the output beam to emerge with several different Stokes- and anti-Stokes-shifted frequencies. We chose a difference frequency mixing scheme with a lithium niobate ($LiNbO_3$) crystal that requires the collinear mixing of a 1.91-µm and a 1.06-µm beam. Therefore, the first Stokes-shifted 1.91-µm output from the Raman cell is mixed with the other 1.06-µm beam in the $LiNbO_3$ crystal to produce the 2.41-µm pump beam. The residual 1.06-µm beam from the conversion process is used as the probe beam and is sent into a variable time delay that consists of a reflective corner cube mounted onto a computer-controlled translation stage. The delay stage allows for precise incremental time delays between the pump and probe beams. The pump and probe beams are independently focused into the sample, and the 0.88-µm emission signal is recorded with a photomultiplier tube placed at the side of the sample. Two independent reference detectors are used to account for fluctuations in the laser output. All three signals from the detectors are

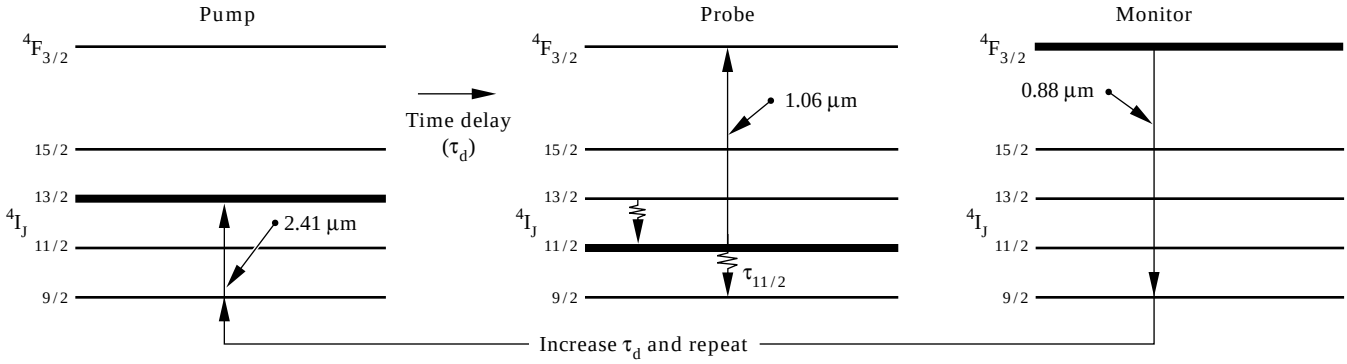

FIGURE 3. The pump-probe experiment. A 2.41-µm pump pulse excites a fraction of the ground state population into the $^4I_{13/2}$ level. After a time delay (τ_d), the 1.06-µm probe pulse excites the Nd ions from the $^4I_{11/2}$ level into the upper $^4F_{3/2}$ level. The 0.88-µm emission corresponding to the $^4F_{3/2} \rightarrow {}^4I_{9/2}$ transition is time integrated and recorded. This sequence of events is repeated for longer time delays. (70-15-0194-0202pb02)

sent into electronic boxcars that integrate the waveforms. A hardware interface allows a computer to store the integrated signals. After the data are stored, the computer translates the delay stage and records a new set of data.

Figure 5 shows an example of the data taken with this setup. The data are illustrated with circles; the line is the numerical model. Details of the numerical model have been described elsewhere.[1] In brief, the model of the data includes information about the $^4I_{13/2} \rightarrow {}^4I_{11/2}$ and $^4I_{11/2} \rightarrow {}^4I_{9/2}$ nonradiative transitions. Three adjustable physical parameters fit the data to the model. We calculated a lower bound of the terminal lifetime by correcting the effective lifetime for the ~200 cm^{-1} smaller gap in the $^4I_{11/2} \rightarrow {}^4I_{9/2}$ transition compared with the $^4I_{13/2} \rightarrow {}^4I_{11/2}$ transition. The terminal lifetime (lower-bound) was found to be 250 ps with an error of ±100 ps.

Indirect Method: Experiment and Results

Before discussing the indirect method, we first briefly explain the energy gap law. The nonradiative rate for the transition of a rare-earth ion such as Nd within a glass or crystalline host medium can be written as

$$W_{nr} = A \exp(-\alpha p) \quad , \tag{1}$$

where A and α are host-dependent parameters and p is the normalized energy gap of the transition, $\Delta E_{gap} / h\nu_{eff}$.

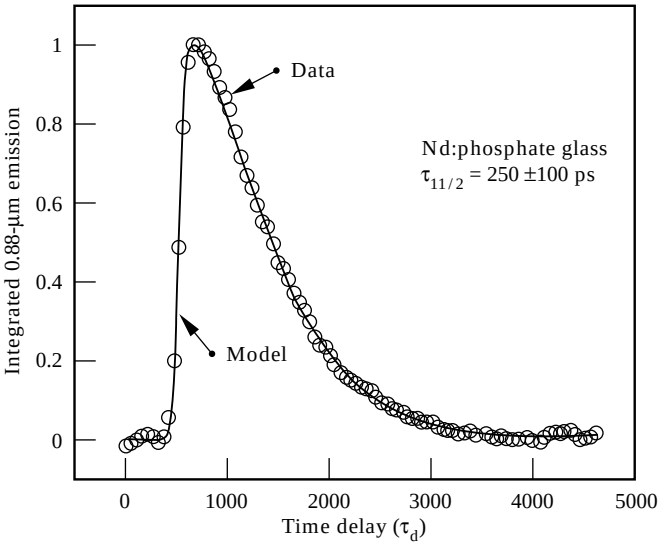

FIGURE 5. The analysis of the data yielded a terminal lifetime of $\tau_{11/2}$ = 250 ps with an error of ±100 ps. (70-15-0194-0202pb04)

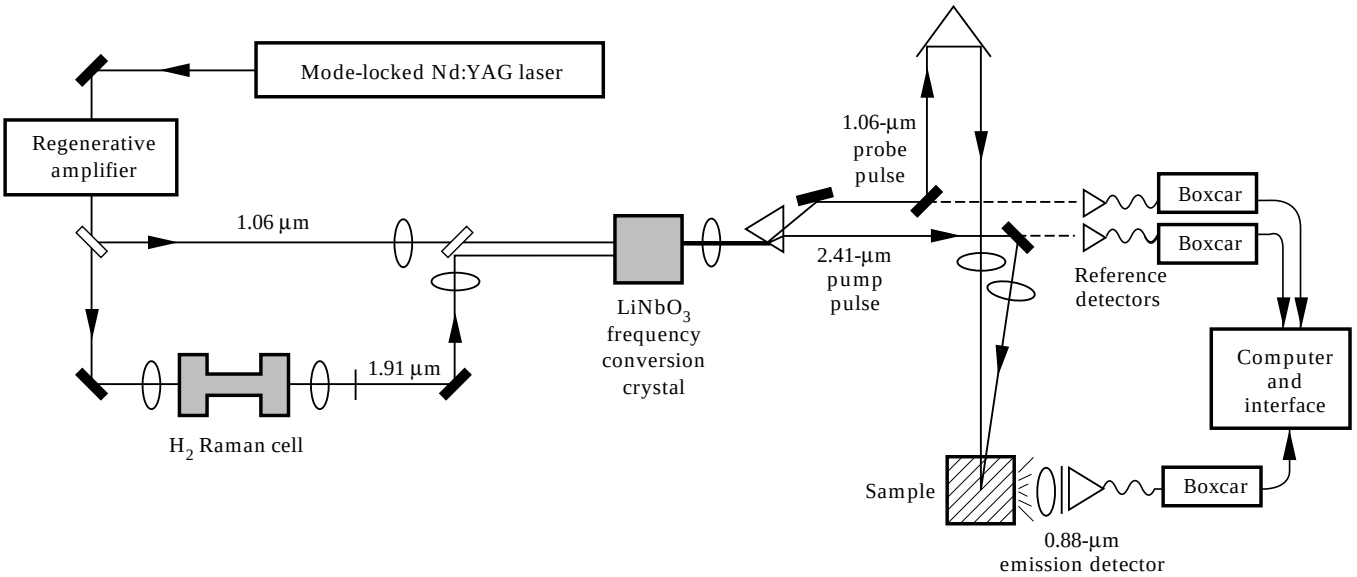

FIGURE 4. A simplified experimental diagram for the pump-probe experiment. The 1.06-µm output of the laser is mixed with the 1.91-µm Stokes-shifted output from an H_2 Raman cell to produce a 2.41-µm pump beam. The residual 1.06-µm beam is delayed and used as the probe beam. Three individual detectors and boxcars record and integrate the signals, which are stored on the computer for subsequent data analysis. (70-15-0194-0202pb03)

This expression assumes that for transitions involving approximately two or more phonons, only the highest frequency of vibration (ν_{eff}) in the host plays a significant role in enabling the nonradiative transition. Therefore the smallest number of high-frequency phonons needed to bridge the energy gap (ΔE_{gap}) tends to dominate the nonradiative decay. In addition, the theory assumes that only the size of the gap is important and not the specific details of the initial and final electronic states over which the transition takes place—hence the reason for the name "energy gap law."

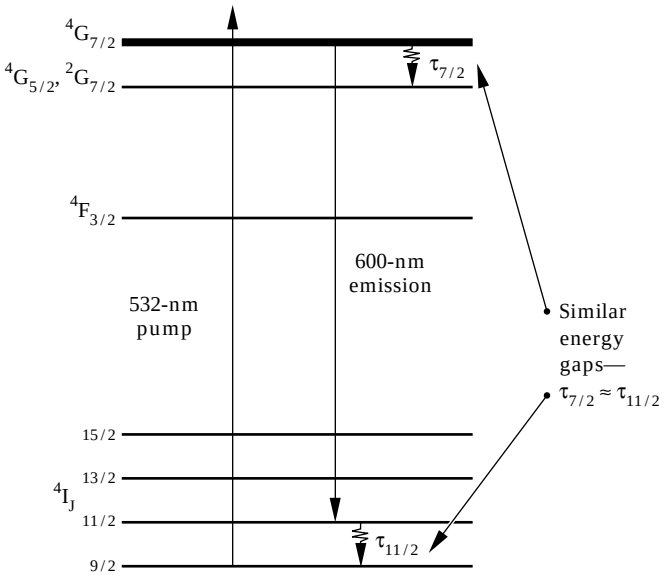

FIGURE 6. An energy level diagram for the emission experiment. A 532-nm pump beam transfers a fraction of the ground state population into the $^4G_{7/2}$ level. The resulting emission at 600 nm from the $^4G_{7/2}$ level is recorded. Since the nonradiative decay for the $^4G_{7/2} \rightarrow {}^4G_{5/2}$, $^2G_{7/2}$ transition will be much faster than the radiative decay rate, the 600-nm emission signal will be a direct measure of the $\tau_{7/2}$ lifetime. (70-00-0295-0391pb01)

For most Nd-doped materials, the upper $^4G_{7/2} \rightarrow {}^4G_{5/2}$, $^2G_{7/2}$ transition and the lower $^4I_{11/2} \rightarrow {}^4I_{9/2}$ transition have a similar-size energy gap. Figure 6 shows the energy level diagram for the pumping and emission processes. If the energy gap theory is assumed valid, then the values of the $\tau_{7/2}$ and $\tau_{11/2}$ lifetimes should also be quite similar. Since the Nd ions are easily excited from the ground state to the $^4G_{7/2}$ level with the frequency-doubled output of a 1.06-μm laser, one must only monitor emission signals from the $^4G_{7/2}$ level for a direct measure of the $\tau_{7/2}$ lifetime. This is because the rate of decay of the emission signal will be largely dominated by the $^4G_{7/2} \rightarrow {}^4G_{5/2}$, $^2G_{7/2}$ nonradiative rate. After exciting the ground-state Nd ions with the 532-nm pump, the 600-nm emission signal corresponding to the $^4G_{7/2}$ population decay is recorded. A technique suitable for measuring time-resolved fluorescence emission spectra characterized by weak signal levels and/or picosecond lifetimes is called "time-correlated single photon counting."

Figure 7 illustrates an experimental scheme for measuring the $\tau_{7/2}$ lifetime that employs a photon counting system. The frequency-doubled output of a mode-locked Nd:YAG laser produces 1 W of 532-nm light with a 90-ps pulse length at a rate of 76 MHz. The 532-nm light is split into two paths. In path 1, the sample is illuminated and the fluorescence is collected and focused into the monochromator. A multichannel plate photomultiplier tube (MCP-PMT) is placed at the output of the monochromator and detects the 600-nm

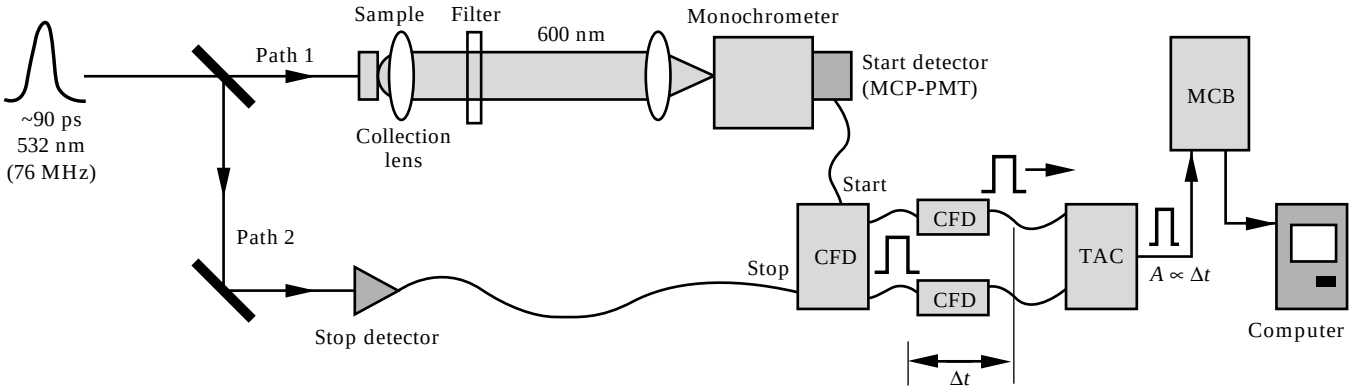

FIGURE 7. An experimental scheme for the emission experiment using a time-correlated single-photon counting technique. The 532-nm pulse is split into two beams. In path 1, a beam illuminates the sample, and the resulting 600-nm emission is detected with a multichannel plate detector. The beam from path 2 is time delayed and focused onto a silicon detector. The photon counting electronics (constant fraction discriminator, time-to-amplitude converter, multichannel buffer) condition the electronic pulses from the two detectors. After multiple excitation pulses, the 600-nm emission waveform is reconstructed. (70-00-0295-0391pb02)

emission signal. The photon counting method assumes that the probability distribution for the emission of the first photon after excitation is also the intensity vs time distribution of the photons emitted as a result of the excitation. Therefore, by measuring the time at which the first photon is emitted for a large number of excitation events, the experiment eventually constructs the full probability distribution.[8] This method uses the high repetition rate of the laser system to build up the emission signal after many excitation pulses.

The sequence of electronic events, as shown in Fig. 7, is as follows: The MCP-PMT monitors the arrival of the first 600-nm photon emitted after the sample has been excited. From the single photon event, the MCP-PMT is able to generate an electronic signal known as the start pulse. The constant fraction discriminator (CFD) conditions the electronic signal from the detectors so that the signals going into the time-to-amplitude converter (TAC) have a precisely timed leading edge independent of the amplitude fluctuations. The pulses entering the TAC initiate the charging of a capacitor. In path 2, the 532-nm pulse is time delayed and sent into a silicon photodetector, which outputs an electronic pulse to stop the charging of the capacitor. The amount of charge stored on the capacitor is proportional to the time interval (Δt) between the start and stop pulses. The TAC outputs an electronic pulse with an amplitude (A) that is directly proportional to the stored charge on the capacitor. A multichannel buffer (MCB) stores the value of the pulse amplitude.

The sequence is repeated until enough single-photon events have been sampled to accurately reconstruct the emission signal. Figure 8 shows the data and model for LG-750. The $\tau_{11/2}$ lifetime inferred from the kinetic analysis is found to be $\tau_{11/2} \cong \tau_{7/2} = 228 \pm 50$ ps on the basis of the $^4G_{7/2} \rightarrow {}^4G_{5/2}$, $^2G_{7/2}$ relaxation time.

Energy Extraction Experiments and Modeling

In 1982, Yarema and Milam[7] performed a series of energy extraction experiments for several Nd-doped glasses, including LG-750. Figure 9 shows a plot of the fluence out vs fluence into an LG-750 amplifier for 1-ns and 20-ns pulse durations. The data show that at higher input fluences, the 20-ns pulses begin to extract the stored energy more efficiently. Based on the experimental values of the terminal lifetime derived from the two experiments previously discussed, we would expect the 20-ns data to extract the energy more efficiently since there is virtually no bottlenecking of the terminal level. This is because the 20-ns pulses are 80 times longer than the terminal lifetime, as opposed to the 1-ns pulses, which are only 4 times longer. The difference in the two data curves can be accounted for by including the terminal-level lifetime in the solution to the coupled population rate and transport differential equations. However, as mentioned earlier, no analytic solution exists, and therefore the equations must be integrated for each new value of the pulse length t_p or the terminal

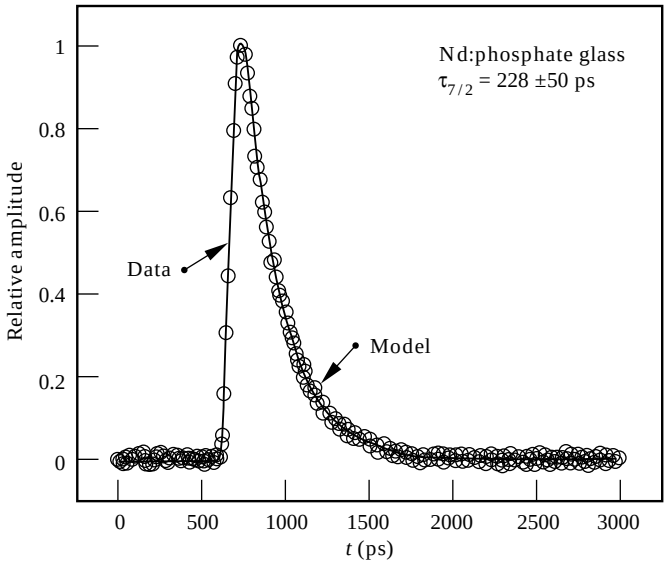

FIGURE 8. A plot of the 600-nm emission as a function of time. The $\tau_{7/2}$ lifetime derived from the data analysis is 228 ± 50 ps. (70-00-0295-0391pb03)

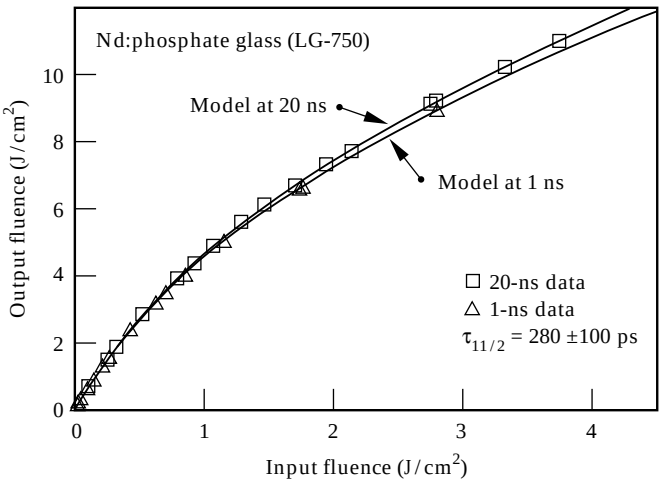

FIGURE 9. A plot of the extraction data taken by Yarema and Milam for 1- and 20-ns square pulses in the phosphate glass composition LG-750. A model that includes the ratio of the pulse width to the terminal-level lifetime is shown as the two solid lines. The terminal-level lifetime was left as a variable fitting parameter within the model. A best fit to the data yielded $\tau_{11/2} = 280 \pm 100$ ps. (70-00-1194-3749pb02)

lifetime $\tau_{11/2}$. We have found an empirical formula for the saturation fluence F'_{sat} that explicitly includes t_p and $\tau_{11/2}$:

$$F'_{sat} = \left[\frac{h\nu / \sigma_{em}}{1 + \frac{g_2}{g_1} B(R)} \right] \quad , \tag{2}$$

where $B(R)$ is a function of $R = t_p / \tau_{11/2}$, σ_{em} is the emission cross section, and g_2/g_1 is the ratio of upper to lower level degeneracies of the laser transition. The derivation of the function $B(R)$ will be discussed in the next section. The empirical formula for the saturation fluence can be substituted within the Frantz–Nodvik[6] solution for energy extraction to model both the 1-ns and 20-ns data. The Frantz–Nodvik solution is written as

$$F_{out} = F'_{sat} \ln\left\{1 + G_0\left[\exp\left(F_{in} / F'_{sat}\right) - 1\right]\right\} \quad , \tag{3}$$

where G_0 is the small signal gain and F_{in} is the input fluence. The model is shown as the curves in Fig. 9. The terminal-level lifetime was left as a fitting parameter within Eq. (3). The best fit to the data yielded a terminal lifetime of $\tau_{11/2}$ = 280 ps ± 100 ps. This result is within the experimental error of the lifetimes derived from the previous sections. The average terminal lifetime and estimated error from all three experiments is 253 ps with an rms error of ±50 ps.

Derivation of the Modified Saturation Fluence

There are six steps involved in finding the functional form of $B(R)$ in Eq. (2).

1. Transform the coupled rate and transport equations that include the terminal-level lifetime ($\tau_{11/2}$) to a coordinate system that moves within the frame of the pulse.
2. Simplify the equations by integrating over the spatial dimension so that only a set of coupled ordinary differential equations in time remain.
3. Integrate the coupled equations for a range of R values.
4. Substitute the modified saturation fluence defined in Eq. (2) into the Frantz–Nodvik solution, Eq. (3), fit each of the empirical output-vs-input fluence solutions to the exact numerical solutions found in step 3, and determine $B(R)$.
5. Find an analytic form for $B(R)$.
6. Determine the range of input parameters over which the modified saturation fluence F'_{sat} can be used.

We begin by assuming that the upper laser level has a population $N_2(0)$ created by a previous pumping process when the input pulse arrives. The coupled rate and energy transport equations for a lossless system can be written as

$$\frac{\partial N_2(t)}{\partial t} = -\frac{I(z,t)}{h\nu}\left[\sigma_{em} N_2(t) - \sigma_{abs} N_1(t)\right] \quad , \tag{4a}$$

$$\frac{\partial N_1(t)}{\partial t} = \frac{I(z,t)}{h\nu}\left[\sigma_{em} N_2(t) - \sigma_{abs} N_1(t)\right] - \frac{N_1(t)}{\tau_{11/2}} \quad , \tag{4b}$$

and

$$\frac{\partial I(z,t)}{\partial z} + \frac{n}{c}\frac{\partial I(z,t)}{\partial t} = I(z,t)\left[\sigma_{em} N_2(t) - \sigma_{abs} N_1(t)\right] \quad , \tag{4c}$$

where $N_2(t)$ and $N_1(t)$ represent the upper ($^4F_{3/2}$) and lower ($^4I_{11/2}$) level populations, σ_{em} is the single-ion stimulated emission cross section for the $^4F_{3/2} \rightarrow {}^4I_{11/2}$ transition, and σ_{abs} is the single-ion absorption cross section for the $^4I_{11/2} \rightarrow {}^4F_{3/2}$ transition. The intensity of the laser pulse is denoted by $I(z,t)$. In a glass, σ_{em}, σ_{abs}, and $\tau_{11/2}$ are supposed to be site-averaged or ensemble values.

Eqs. (4a)–(4c) can be simplified by transforming them to a moving coordinate system that travels at the velocity of the pulse by making the following transformation of variables: $T = t – (zn/c)$ and $Z = z$. Using the prescription of Trenholme et al.[9] we also define $\beta = N_2\sigma_{em}$ to be the gain coefficient of the upper level ions and $\alpha = N_1\sigma_{abs}$ to be the absorption coefficient of the lower level ions. The ratio of degeneracies is defined to be the constant $K = \sigma_{abs} / \sigma_{em}$. The result is

$$\frac{\partial \beta}{\partial T} = -\frac{I}{h\nu / \sigma_{em}}\left[\beta - \alpha\right] \quad , \tag{5a}$$

$$\frac{\partial \alpha}{\partial T} = \frac{IK}{h\nu / \sigma_{em}}\left[\beta - \alpha\right] - \frac{\alpha}{\tau_{11/2}} \quad , \tag{5b}$$

and

$$\frac{\partial I}{\partial Z} = I\left[\beta - \alpha\right] \quad . \tag{5c}$$

Eqs. (5a)–(5c) can be further simplified by observing that integration over their spatial dimension is possible, leaving a set of ordinary differential equations in time to be solved. Continuing to follow Trenholme, the quantities $U(t)$ and $L(t)$ are defined as

$$U(t) = \int_0^{\ell} \beta(z,t)\, dz \tag{6a}$$

and

$$L(t) = \int_0^{\ell} \alpha(z,t)\, dz \quad . \tag{6b}$$

Integrating Eqs. (5a)–(5c) along the length of the amplifier, we find that the problem now reduces to solving the following set of coupled differential equations of Trenholme[9]:

$$\frac{dU}{dt} = -\frac{I_{\text{in}}\left(e^{U-L}-1\right)}{h\nu/\sigma_{\text{em}}} \quad , \tag{7}$$

$$\frac{dL}{dt} = \frac{I_{\text{in}}K\left(e^{U-L}-1\right)}{h\nu/\sigma_{\text{em}}} - \frac{L}{\tau_{11/2}} \quad , \tag{8}$$

and

$$\frac{dF_{\text{out}}}{dt} = I_{\text{out}} = I_{\text{in}}e^{U-L} \quad , \tag{9}$$

where the known initial conditions $U(0)$, $L(0)$, and $I_{\text{in}}(t)$ are used to integrate Eqs. (7)–(9) forward in time. The integrated output intensity yields the output fluence

$$F_{\text{out}}(\text{numerical}) = \int_0^{\infty} I_{\text{out}}(t)\, dt = \int_0^{\infty} I_{\text{in}}(t)\, e^{U-L}\, dt \quad , \tag{10}$$

where F_{out} (numerical) is the exact solution to the lossless coupled rate and energy transport equations that includes effects of the terminal-level lifetime ($\tau_{11/2}$). The numerical solutions of Eq. (10) for square pulses with $R = t_p/\tau_{11/2} = 0.01$, 2, and 100 are plotted in Fig. 10(a). For each numerical solution shown, a best fit of the empirical solution, Eq. (3), was found by adjusting the value of $B(R)$ to minimize the χ^2 fitting error. The empirical solutions are also shown in Fig. 10(a) along with the corresponding $B(R)$ and χ^2 values where we define

$$\chi^2 = \sqrt{\sum_{i=1}^{N=100} \left[F_{\text{out}}^{\text{num}}(i) - F_{\text{out}}^{\text{emp}}(i)\right]^2 \frac{1}{N-1}} \quad . \tag{11}$$

In Fig. 10(a), only three different values of $B(R)$ were determined. To find a functional form for $B(R)$, additional values were needed. In Fig. 10(b), over 1000 fits are shown to produce a nearly continuous curve for $B(R)$ (solid line). As required, $B(R)$ converges to the asymptotes of 1 and 0 for $t_p/\tau_{11/2} << 1$ and $t_p/\tau_{11/2} >> 1$, respectively. The $B(R)$ curve shown in Fig. 10(b) was fit to three exponentials (open circles). This allowed for an improved fit to the $B(R)$ curve compared with the single exponential form originally proposed by Trenholme.[10] The exponential sum is written as

$$B(R) = a_1 \exp\left(-R/b_1\right) + a_2 \exp\left(-R/b_2\right) + a_3 \exp\left(-R/b_3\right) \quad , \tag{12}$$

where the coefficients are

$$a_1 = 0.59735, a_2 = 0.34025, a_3 = 0.0605 \tag{13a}$$

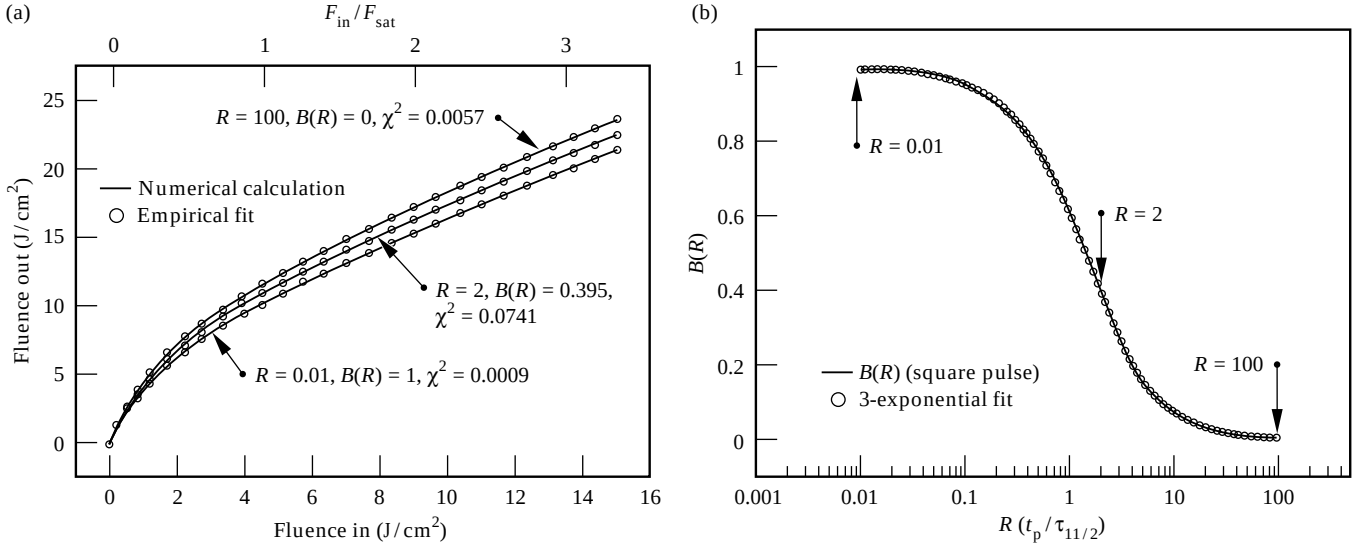

FIGURE 10. (a) A plot of the numerical solution of the coupled differential equations, Eq. (10), is shown as the solid line. The open circles represent the empirical solution, Eq. (3). The value for $B(R)$ and the χ^2 fitting error are also shown. (b) Over a thousand fits, such as those shown in (a), were made to form a nearly continuous curve for $B(R)$. A best fit to the curve for a sum of three exponentials is shown by the open circles. (70-00-0295-0393pb01)

and

$$b_1 = 1.29348, b_2 = 4.14937, b_3 = 30.38384 \quad . \tag{13b}$$

To match the experimental data, Eq. (12) was evaluated for the following input parameter values:

$$g_2 / g_1 = 0.35 \quad , \tag{14a}$$

$$G_0 = 6.9 \quad , \tag{14b}$$

and

$$I_{\text{in}}(t) = I_0 \exp\left[-(t / w)^{30}\right] \quad , \tag{14c}$$

$I_{\text{in}}(t)$ being a square pulse approximated by a super-Gaussian of power 30. In addition, the relevant range of input fluences are defined with

$$\frac{F_{\text{in}}}{h\nu / \sigma_{\text{em}}} < 3.5 \quad . \tag{14d}$$

The empirical expression for the saturation fluence, Eq. (3), with $B(R)$ defined in Eq. (12), can be used to calculate the output energy with an error of less than 1.5%. Our choices for the value of the parameters—g_2 / g_1, G_o, and $I_{\text{in}}(t)$—and therefore $B(R)$ are specific to Yarema and Milam's extraction experiment. Equation (12) has some applicability for alternative ranges of input parameters.[11]

In a recent publication by Beach et al.,[12] an approximate form for $B(R)'$ was derived and shown to be

$$B(R)' = \frac{1 - \exp(-R)}{R} \quad . \tag{15}$$

However, Eq. (15) proved to be useful only for input fluences less than the saturation fluence of the medium ($F_{\text{in}} < h\nu / \sigma_{\text{em}}$). We have nonetheless found that an adequate fit to $B(R)$ can be achieved over a larger F_{in} range if an additional phenomenological parameter is introduced by taking the entire expression to the 1.13 power (i.e., $[B(R)']^{1.13}$). By substituting this alternative form of $B(R)$ into Eq. (2), we can determine the output energy with an error of less than 1.5% for the input parameters in Eqs. (14a)–(14c).

Comparison of the Direct and Indirect Methods for Several Nd-Doped Materials

We have discussed three possible experiments for measuring the terminal lifetime for Nd:phosphate glass. It would be convenient if the simplest method were shown to be sufficiently accurate for measuring the terminal lifetime of any Nd-doped laser material. Table 1 lists lifetime data for 13 different Nd-doped laser materials taken from the pump-probe and emission experiments previously discussed. In Fig. 11, the lifetime from the direct data ($\tau_{11/2}$) is plotted against the lifetime from the indirect method ($\tau_{7/2}$). The figure shows a line representing the best fit to the data of the form $y = mx$. Ideally, if both methods yielded the same results, then the slope m would be equal to one. However, the best fit produced a slope of 1.15, which suggests that the simpler, indirect method can be used to determine the terminal-level lifetime for most Nd-doped materials within a factor of two provided that the excitation pulses are short enough and the detectors and electronics have the required sensitivity and resolution.

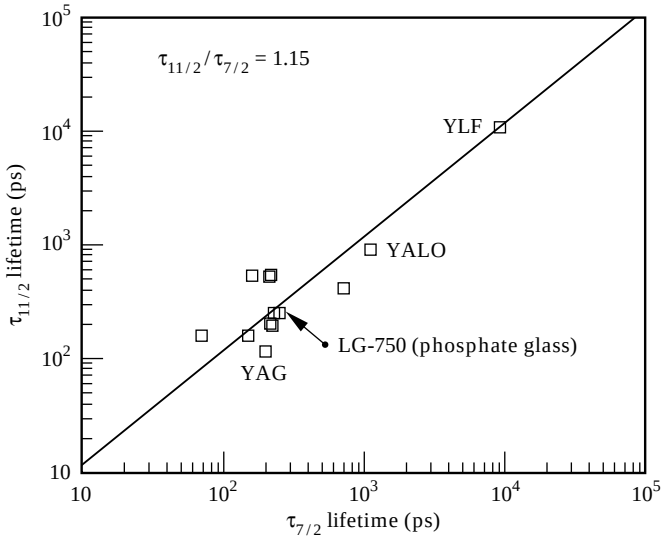

FIGURE 11. The terminal lifetimes from the direct and indirect measurements are plotted. A best fit to the data is shown as the solid line of the form $y = mx$. The slope is 1.15. We find that the indirect method can be used to measure the terminal lifetime to within a factor of 2 for most Nd-doped laser materials. (70-00-0295-0394pb01)

The rightmost column of Table 1 lists our best assessment of the terminal lifetime from the two approaches. In comparing the lifetimes of the various groups of materials, we find that the phosphate glasses have a factor-of-two shorter lifetime than the silicate glasses. This is primarily due to the high phonon frequencies of the network forming PO_4 complexes in the phosphate host as opposed to the relatively low-frequency SiO_4 complexes in the silicate glasses. The shortest lifetime measured was from the phosphate crystal Nd:C-FAP. This material has both high phonon frequencies and a small energy gap. Within the oxide crystals, we find that Nd:YAG has the shortest lifetime and correspondingly the smallest energy gap. And finally, as expected, we find that for the fluoride materials, including Nd:YLF, the relatively low 300–600 cm^{-1} phonon frequencies give rise to slower (nanosecond) lifetimes.

Conclusions

We measured the terminal-level lifetime of the Nd-doped phosphate glass LG-750 from three independent measurements and found the average value to be $\tau_{11/2}$ = 253 ps with an rms error of ±50 ps. In the process of modeling data from the energy extraction experiments, we developed an empirical formula for the saturation fluence that can be used to account for the bottlenecking effects of the $^4I_{11/2}$ level in the Frantz–Nodvik analytic solution for energy extraction. We determined that the indirect emission measurements yield lifetimes that are within a factor of two of the direct pump-probe measurements. This result gives us confidence in using the simpler indirect approach for estimating the terminal lifetime for new prospective Nd-doped laser materials.

TABLE 1. Results from the direct, pump-probe measurements and the indirect, emission measurements. The right column lists our best assessment of the terminal lifetimes.

Material	Lifetime $\tau_{11/2}$ (ps)	Lifetime $\tau_{7/2}$ (ps)	Best assessment of lower-level lifetime (ps)
Phosphate glasses			
LG-750	250	228	250[a]
APG-1	192	215	192[a]
APG-x	200	210	200[a]
APG-y	158	150	158[a]
Phosphate crystal			
C-FAP, $Ca_5(PO_4)_3F$	156	70	70[b]
Silicate glasses			
LG-660	535	215	535[c]
LG-650	510	210	510[c]
SOL-GEL	247	245	247[a]
Oxides			
YAG, $Y_3Al_5O_{12}$	115	200	200[b]
YALO, $YAlO_3$	896	1090	1090[b]
GSGG, $Gd_3Sc_2Ga_3O_{12}$	401	715	715[b]
Vanadate			
YVO_4	531	190	531[d]
Fluorides			
YLF, $LiYF_4$	10,500	9100	9100[b]
SrF_2	>5000	7000	7000[b]
Fluoride glass			
ZBLAN, ZrF_4-BaF_2-AlF_3-LaF_3-NaF	>5000	18,000	18,000[b]

[a] Lower limit of the lifetime from the direct method agrees with the lifetime measured from the indirect method.

[b] Indirect method is preferred since data is more accurate.

[c] Energy gap relevant to $^4I_{11/2}$ and $^4G_{7/2}$ states are anomolously different so the $\tau_{11/2}$ and $\tau_{7/2}$ lifetimes do not agree.

[d] Basis for difference between the $\tau_{11/2}$ and $\tau_{7/2}$ lifetimes is uncertain.

Acknowledgments

We thank John Trenholme for sharing his insights into modeling this process with his laser extraction code and for his helpful editorial suggestions. We also thank Howard Powell for emphasizing the need for a direct experimental measurement of the terminal-level lifetime. We thank Ray Beach for his helpful discussions and notes on the derivation of the extraction efficiency of Nd:YLF. We also recognize Steve Velsko, Chris Ebbers, Mark Hermann, and Laura DeLoach for their help with the frequency conversion scheme, Chris Marshall for helping with the photon counting system, Joel Speth for supporting the laser systems, Gary Wilke for assistance with the spectroscopy, and Ron Vallene and Peter Thelin for preparing the samples. In addition, we thank Bill Krupke for his helpful discussions on the material physics issues and Ann Orel for periodically reviewing the progress on this project. We also extend our appreciation to Wolfe Seka and Jonathan Zuegal of the University of Rochester[13] for initially sharing an alternative approach for measuring the Nd terminal-level lifetime, and to Schott Glass, Inc.[14] for the LG-750 phosphate glass.

Notes and References

1. C. Bibeau, S. A. Payne, and H. T. Powell, "Evaluation of the Terminal-Level Lifetime in Sixteen Neodymium-Doped Crystals and Glasses," Lawrence Livermore National Laboratory, Livermore, CA, UCRL-JC-117099 (1994).
2. L. A. Riseberg and H. W. Moos, *Phys. Rev*. 174, 429–438 (1968).
3. C. B. Layne, W. H. Lowdermilk, and M. J. Weber, *Phys. Rev. B* 16, 10–20 (1977).
4. L. M. Frantz and J. S. Nodvik, *J. Appl. Phys.* 34, 2346–2349 (1963).
5. S. M. Yarema and D. Milam, *IEEE J. Quantum Electron*. QE-18, 1941–1946 (1982).
6. W. E. Martin and D. Milam, *Appl. Phys. Lett.* 32, 816–818 (1978).
7. K. Palombo, S. Matthews, S. Sheldrake, and C. Capps. *OSA Proc. on Advanced Solid-State Lasers* 15, 78–80 (1993).
8. D. V. O'Connor and D. Phillips, *Time-Correlated Single Photon Counting* (Academic Press, 24–28 Oval Rd., London, NW1 7DX, 1984).
9. J. B. Trenholme and E. J. Goodwin, "Numerical modeling of gain recovery," *Laser Program Annual Report* 1, 2.236–2.238, Lawrence Livermore National Laboratory, Livermore, CA, UCRL-50021-77 (1977).
10. J. Trenholme, J. Hunt, and J. Murray, Lawrence Livermore National Laboratory, "Assumptions which produced the upgrade design," Internal memorandum, LS&T 91-65 (1991).
11. C. Bibeau, J. B. Trenholme, and S. A. Payne, "Pulse length and terminal level lifetime dependence of energy extraction for neodymium-doped phosphate amplifier glass," Lawrence Livermore National Laboratory, Livermore, CA, UCRL-JC-120909, to be published in *IEEE J. Quantum Electron*.
12. R. Beach et al., *Opt. Lett.* 18, 1326–1328 (1993).
13. University of Rochester, Rochester, New York, 14623–1299.
14. Schott Glass Technologies Inc., 400 York Ave., Duryea, PA, 18642.